Diamond & Related Materials 159 (2025) 112726

Contents lists available at ScienceDirect

Diamond & Related Materials

journal homepage: www.elsevier.com/locate/diamond

Tribological Properties of Diamond–Silica Interfaces: Effects of surface termination, orientation and boron doping

Stefanos Giaremis [a], Huong Ta Thi Thuy [a], Mauro Ferrario [b], Maria Clelia Righi [a,*]

[a] Department of Physics and Astronomy, University of Bologna, 40127 Bologna, Italy
[b] Dipartimento di Scienze Fisiche, Informatiche e Matematiche, Università di Modena e Reggio Emilia, Via Campi 213, /A, 41125 Modena, Italy

ARTICLE INFO

Keywords:
Boron-doped diamond
Diamond coatings
Tribology
Ab initio molecular dynamics calculations

ABSTRACT

The diamond–silica interface is a system of high technological relevance and constitutes an ideal platform for assessing the effects of surface chemistry and dopants on adhesion, friction, and wear. In this work, we employed *ab initio* molecular dynamics simulations for evaluating the impact of different diamond surface terminations and orientations, along with boron (B) doping, on the tribological behavior of the diamond–silica interface. The F-termination resulted as the most effective among those considered in reducing the adhesion and friction, making all the diamond surfaces inert. On the other hand, B-doping was found to enhance the diamond surface reactivity, interfacial adhesion and wear. Among the considered surface orientations, the Pandey-reconstructed C(111) surface, turned out to be the most slippery and the C(110) the most prone to wear.

1. Introduction

Diamond, as the hardest known material and also thanks to its low friction and high stability, is extensively used in applications such as protective coatings, micro/nanoelectromechanical switches (MEMS/NEMS), ultrahigh precision machining tools, atomic force microscopy (AFM) probes and others [1–3].

However, the tribological properties of diamond coatings are dependent on various factors such as the environmental conditions, the surface termination and the type of counter-surface and substrate. More specifically, higher friction, wear rates and material loss have been reported from tribological experiments on diamond coatings in dry or vacuum conditions [4–7]. These effects have been attributed to increased adhesion due to surface dangling bonds, at variance with what happens in humid conditions where they can be effectively passivated by H or OH species, that are produced by the tribochemically induced dissociative adsorption of ambient molecules [8–11]. Indeed, while hydrogenated diamond films have been shown to yield ultralow friction [12–15], at the same time there is also evidence that this behavior exhibits only short-term stability [16,17]. Joint H and OH terminations were conversely found to yield improved stability and friction under load [17] and also alternative terminations with fluorine has been explored, since F atoms, larger and more electronegative than H atoms, are more strongly bound to C atoms and can promote steric effects and Pauli repulsion with the countersurface [18–21]. Similarly, oxygen terminations have been shown to increase surface separation and to reduce friction compared to hydrogen terminations in diamond–silica interfaces and also to lead to ultralow friction between diamond surfaces [11,22,23]. Oxidation in the form of C-O or C=O terminating species has been experimentally observed [8,24] and it is expected under ambient conditions, since the dissociation of oxygen molecules has a lower energy barrier compared to hydrogen and water ones, as shown from *ab initio* calculations [25].

Furthermore, doping with B has been widely explored for further enhancing the mechanical properties of diamond films. For instance, diamond coatings in cemented tungsten carbide-based (WC-Co) cutting tools often suffer from poor adhesion and shedding due to Co-catalyzed graphitization at the interface and the mismatch in thermal expansion coefficients between WC-Co and diamond [26,27]. B atoms have a larger covalent radius than C atoms and reduce the amount of weak C–C sp^2 bonds, while also creating tensile stress in the diamond layer that mitigates the compressive residual stress from the WC-Co substrate [28–31]. Moreover, B adatoms have been shown to increase adhesion in metal–metal and diamond–metal interfaces [32,33]. Many experimental studies report that B doping in diamond-based coatings has an overall positive effect in many applications by reducing friction and improving substrate adhesion, wear resistance and biocompatibility [29–31,34,35]. However, there are as well evidences that link B doping to reduced hardness and increased wear rates [35–39]. Direct evaluation at the atomistic level of the seemingly ambiguous impact

* Corresponding author.
E-mail address: clelia.righi@unibo.it (M.C. Righi).

https://doi.org/10.1016/j.diamond.2025.112726
Received 16 May 2025; Received in revised form 22 July 2025; Accepted 7 August 2025
Available online 16 August 2025

of B doping in diamond coatings is complicated by the interplay of the many different parameters, such as substrate and counter-surface materials, grain size and working environments, all simultaneously present in the above mentioned experiments.

The diamond–silica interface is a system that is highly relevant for many technological applications. The process of chemical mechanical polishing (CMP) is an emerging technique for smoothing diamond surfaces, introducing minimal damage and defects [40,41]. CMP involves the use of a silica-based colloidal containing silanol groups ($Si(OH)_4$) which become attached to atoms at the diamond surface and consequently removes them when shearing mechanical forces are applied [40,41]. Results of semi-empirical and classical molecular dynamics (MD) simulations have suggested that the wear mechanism is initiated via the formation of strong C-Si and C-O bonds between diamond and silica, and manifests in various forms, such as atom-by-atom, carbon chains, sheets and graphitization [22,23,42–45]. Other systems in which the diamond–silica interface is relevant are AFM and scanning microscopy tips and MEMS/NEMS devices [46,47]. Furthermore, thanks to the rich variety of chemical interactions occurring at its interface, this system offers, besides its technological interest, an interesting platform for experimentally and theoretically assessing wear and more generally the tribological behavior of diamond-based systems [42,43,47]. For instance, the reduction of friction and adhesion between silica and diamond when the latter is passivated with O and H has been demonstrated by *ab initio* molecular dynamics (AIMD) simulations by our group [22,23].

In this work, we explore the impact of different terminations, different surface orientation and of B-doping on the tribochemistry occurring at the diamond–silica sliding interface. Specifically, for the (100), (110) and Pandey reconstructed (111) orientations, which are the most commonly exposed facets in diamond films, we explore the behavior of both clean surfaces, corresponding to dry sliding, and partial H, O, H_2O and F terminations, which are likely to arise in various ambient environments or passivation strategies. We employ AIMD simulations under tribological conditions [10] with models of ~400 atoms and simulation times of ~25 ps to obtain a realistic description of the involved systems and interactions, and to directly compare the results with previous works performed by our group [22,23]. Our results aim to improve the current understanding of the main mechanisms governing the interactions at the diamond–silica interface, as well as the impact of different passivations and B-doping to the tribological and mechanical properties of diamond coatings, relevant in numerous technological applications.

2. Computational details

Calculations were performed by using Quantum ESPRESSO [48,49] with the ultrasoft Vanderbuilt pseudopotentials for the expression of the exchange–correlation functional based on the Perdew, Burke and Ernzerhof (PBE) derivation of the generalized gradient approximation (GGA) [50–52]. The wavefunction and charge density cutoff energies were set to 30 and 240 Ry, respectively. To account for the long-range Van der Waals interactions, we employed the semi-empirical D2 dispersion correction of Grimme [53,54]. Spin polarization was enabled to properly describe the potential presence of magnetization from dangling bonds or bond-breaking events. The Brillouin zone was sampled at the Γ point and simulations were performed for times long enough to capture the tribochemical effects of interest. The force and total energy thresholds for relaxations, and the total energy threshold for the electronic self-consistent cycle were set to 10^{-4} a.u., 10^{-5} Ry and 10^{-6} Ry, respectively. All the above approaches and parameters were chosen after extensive testing in our previous works for representing diamond–silica sliding interfaces [22,23], and they were employed in this study to allow for a direct comparison.

Regarding the diamond–silica interface, we considered three different diamond surfaces, namely the C(110), dimer-reconstructed C(001) and Pandey-reconstructed C(111), which are commonly observed experimentally in facets and have also been previously used in similar studies by our group [22,23], thus allowing for direct comparisons. The choice of using reconstructed surface models is in line with previous evidence of graphitization and rehybridization in diamond coatings in tribological conditions [55]. More detailed information about the structure of the diamond slabs can be found in Ta et al. [22]. The lateral dimensions of the systems were $10.119\ \text{Å} \times 17.887\ \text{Å}$ for the systems involving the C(110) and the C(001) surfaces and $10.119\ \text{Å} \times 8.763\ \text{Å}$ for the systems involving the C(111) surfaces. To examine the impact of B doping to the tribochemical behavior of the system, since B is preferably located in substitutional sites at the topmost surface layer [56–58], we have substituted 3, 4 and 2 C atoms with B ones from the topmost layer of the C(110), C(001) and C(111) surfaces, respectively. This corresponds to a total B concentration of 1.50 *at.* %, 1.68 *at.* % and 1.32 *at.* % at the bulk for each case.

To further assess the impact of different surface terminating species, besides the clean surfaces, H, O, H_2O and F terminations at 50% coverage were considered for both undoped and B-doped systems. Partial terminations were considered for examining realistic sliding conditions, which can involve mixed passivated and unpassivated regions of the coating. Moreover, our previous calculations have shown that interfaces involving fully passivated diamond surfaces with H, O and OH do not involve bonding interactions, leading to large interfacial separations and in turn to low adhesion and friction [14,22,23,59]. The H_2O termination involves surface passivation with H and OH fragments assumed from the dissociation of H_2O molecules. While previous *ab initio* studies have shown that H_2O molecules can be undissociatevely chemisorbed on B-doped diamond surfaces via the formation of dative B-O bonds [57,58], this is expected to be highly unlikely to occur in harsh tribological conditions, as it has also been shown that H_2O rapidly dissociates at sliding diamond interfaces, in the same conditions as we examine here [23]. Moreover, there is previous evidence showing that surface B dopants can reduce the energy barriers for H_2O dissociation on diamond surfaces [58]. Therefore, we assume that the dissociative adsorption of H_2O would be the most representative scenario. For the B-doped systems, the energetically preferable configurations for the dissociated molecules from [58] were considered for the sites of the terminating species. The results for the undoped O- terminated cases were obtained from [22]. The B-doped diamond surface configurations are shown in Fig. 1.

The amorphous silica models for the countersurface were developed as described in our previous works [22,23], and contain silanol (Si–OH) and siloxane (Si–O–Si) terminations, arising from the interaction of silicon oxide with the environment. The model was created by thermally annealing an α-quartz crystalline supercell with a classical force field [60], cutting perpendicular to the lateral dimensions to extract a thin film and passivating Si-O and Si dangling bonds with H and OH, respectively. The silanol density ($4.8\ \text{OH/nm}^2$) and the overall chemistry of the amorphous silica surface models were determined in such a way to reproduce experimental descriptions as close as possible within the scale of quantum calculations [23]. More details regarding the characterization of the silica slabs can be found in [23].

All systems were initially relaxed under a normal load of 1 GPa, applied on the topmost Si atoms of the silica slab perpendicularly to the interface with a direction pointing towards the diamond slab. This choice allows for a direct comparison with our previous AIMD results [22,23], which were performed at the same applied normal load and overall computational parameters. It represents a typical value for simulating tribological processes in systems involving silica as it is well below experimentally reported thresholds for plastic deformation [62] and falls within the range of typical loads used in nanotribological experiments [63]. The interaction energies, E_{ads}, of the systems at this stage were calculated via:

$$E_{int} = E_{diam,sil} - (E_{diam} + E_{sil}) \quad (1)$$

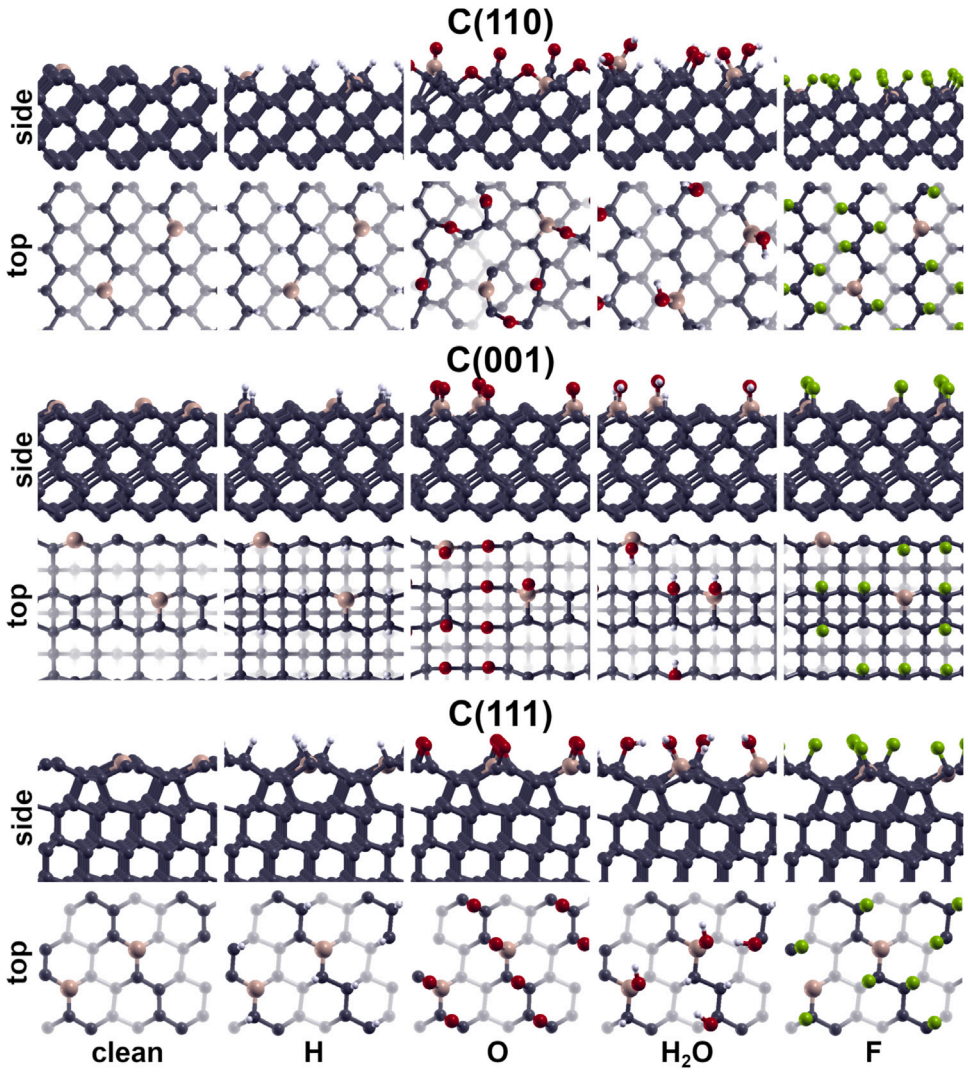

Fig. 1. Top and side view representations of the structural models for the B-doped diamond systems used in this work. Color scheme: C: dark gray, B: pink, H: white, O: red, F: green. The XCrySDen [61] package was used for the visualization of atomic configurations.

where $E_{\mathrm{diam,sil}}$ is the energy of the diamond–silica interface and E_{diam}, E_{sil} the energies of the relaxed isolated diamond and silica slabs, respectively. We considered the most stable geometries starting from four different lateral relative positions of the two slabs.

Subsequently, AIMD calculations were performed on the relaxed structures to simulate the sliding procedure, by using a modified version of the Born Oppenheimer molecular dynamics implementation of the Quantum Espresso package, described in detail in [10], that permits to impose a relative, constant velocity, sliding motion between two independently thermostatted slabs. The Verlet algorithm with timestep of 20 a.u. (~1 fs) was employed. The temperature was set at 300 K by means of a rescaling procedure applied to the atomic thermal velocities. The considered systems were equilibrated for 1 ps and then the silica slabs were set in a constant velocity sliding motion, relative to the diamond slab, for 25 ps. The size of the lateral system dimensions allows for the representation of a large enough interfacial area for sampling tribochemical interactions under load and shear. The duration of the simulations under sliding condition were increased with respect to our previous calculations to ensure reasonable averaging times in stationary conditions, and more statistical robustness within feasible computational costs. A sliding constant velocity of 200 m/s along the x-direction was imposed to the uppermost Si atoms of the silica slab, while keeping fixed the positions of the bottom-most carbon atoms of the diamond slab. The choices of the applied load and temperature are representatives of the typical sliding conditions and allow for direct comparisons with our previous results [22,23].

For quantitatively monitoring the behavior of the interfaces during sliding, the interfacial distance and resistive force for each system were estimated at each timestep. The interfacial distances were calculated by subtracting the average z-coordinates of the C and Si atom innermost layers for each interface, while the resistive friction forces were calculated by summing the x-components of the force exerted on the Si atoms which move at constant velocity and to which the external load was applied [10,22,23]. The averaging and error estimation of the above quantities were performed by the block average technique used in [64].

3. Results and discussion

3.1. Static DFT calculations

We first performed 'static' DFT calculations to obtain an early picture of the behavior of the relaxation of the considered interfaces under pressure. The calculated interaction energies as a function of the interfacial distance for the relaxed systems under a load of 1 GPa are presented in Fig. 2, with the respective relaxed structures included in Supporting Information, Figure S1. The positive sign of the interaction energy observed in all cases (see Fig. 2) indicates a repulsive interaction

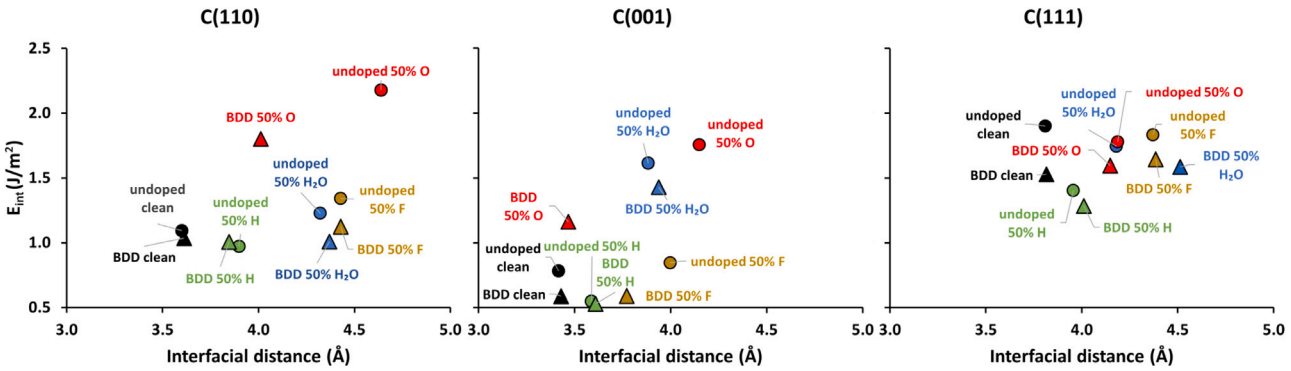

Fig. 2. Interaction energies, E_{int} as calculated via Eq. (1), plotted versus the equilibrium interfacial distance, for the C(110) (left), C(001) (middle) and C(111) (right) surfaces. Black, green, red, blue and yellow notation corresponds to the systems involving clean and 50% H-, O-, split H_2O- and F-terminated diamond surfaces, respectively, while circles denote systems involving undoped diamond surfaces and triangles B-doped ones.

between the diamond and the silica slabs, occurring as the latter is being pushed onto the former. Points higher in each subplot indicate interfaces exhibiting stronger repulsive forces. Similarly, points towards the right side of each subplot correspond to systems with larger interfacial separations. Typically, the interfacial distance becomes larger when adhesive friction becomes lower, so achieving higher repulsion and interfacial separations are beneficial for reducing friction and wear.

Regarding B doping, in most cases, lower values of the interfacial distance and of the interaction energy are found for the B-doped systems compared to their undoped counterparts, as silica can be pushed closer to the diamond surface and at a lower energy cost. This could indicate higher adhesive friction during sliding.

With regard to the impact of the different terminations, 50% H_2O- and F-terminations appear to lead to the largest interfacial separations for either the undoped or the B-doped diamond surfaces. Besides being caused by steric effects, larger interfacial separations often signify stronger repulsive interactions, which typically lead to lower friction and adhesion between sliding surfaces. This is evident for the F-passivated cases, in which larger interfacial separations were observed compared to the H-terminated ones, even with C-F and C-H bonds exhibiting similar lengths. This observation is also in line with the high efficiency of fluorinated lubricants. On the other hand, regardless of doping, the smallest values of interfacial distance and repulsion energy are observed for the clean and the 50% H-terminated diamond surfaces. In such systems, the presence of friction is expected to be more prevalent in tribological conditions.

As for surface orientation, finally, in all cases, the largest interfacial separations and stronger repulsive interactions were found for the C(111) surface, in agreement with its well-known inert character, thus showing its promising character for reducing wear and friction.

Overall, the exploration under load of the minimum energy configurations with static DFT calculations lead to only non-bonded physical interactions present at the diamond–silica interface (Supporting Information, Figure S1). This happened in all cases with the unique exception of the B-doped 50% O-terminated C(001) interface, in which a Si-O-C bond was formed at the interface. While some evidence associating increased adhesion with B-doping, clean and H-terminations and increased separation (and lower adhesion) with H_2O and F terminations and the Pandey C(111) orientation, still not so clear trends were obtained regarding the impact of termination, doping and surface orientation onto the properties of the diamond surfaces.

3.2. Ab initio molecular dynamics calculations

We expect based on previous atomistic-level knowledge that the main mechanisms of friction and wear in the silica–diamond interface during sliding conditions are mainly governed by tribologically-induced bond breaking and reforming events at the sliding interface [22,23,42–45]. Thus, starting from the relaxed structures (Figure S1) obtained in the previous step, we employed AIMD calculations under applied load and shear to capture the "richer" dynamic behavior of the considered diamond surfaces.

Moreover, our approach, as described in Computational Details Section, allows for the direct evaluation of the impact onto friction and wear of the different parameters that we considered in this study. In particular, we can record the full timeseries of the resistive forces per area and of the interfacial distance. Their behaviors for all the considered passivations of the C(110) surface are shown in Fig. 3(a). Their dynamical evolution can be correlated to the tribochemical events that occur during sliding, in particular when a deviation from a stationary behavior occurs for the resistive forces and interfacial distances over time. For instance, the B-doped C(110)-silica interface with 50% O termination exhibited strong bonded interactions immediately from the early stages of the sliding AIMD calculations. These events lead to a drop in the interfacial distance and a corresponding increase in the resistive force already slightly before 5 ps, with the following period characterized by larger fluctuations than in the undoped case. The time series for all the considered systems and conditions are compared in the Figures S2 and S3 in the Supporting Information. The averaged resistive force per area versus the averaged interfacial distance for each surface orientation are presented in Fig. 3(b) and the same quantities, distinct for per termination type, averaged over all three orientations are summarized in Fig. 4.

The impact of B-doping is evident here, as in most cases, B-doped interfaces are associated to higher friction and smaller interfacial separations compared to their undoped counterparts, while also being more prone to wear, as it will be shown in more detail in the following sections.

As expected, in agreement with previous evidences of high friction in diamond coatings under dry conditions [4–7], the highest values of the averaged resistive force are observed for the clean surfaces. On the other hand, partial F termination lead consistently to the lowest values of friction and to the largest values of the interfacial distance, followed in most cases by the partial H_2O termination. Partial O termination, while relatively beneficial for the undoped systems, was found to lead to high friction and wear in the B-doped ones. Finally, partial H terminations in most cases yielded inferior results compared to the rest of the considered types, and specifically compared to the partial F and H_2O terminations.

Regarding the impact of surface orientation, while C(110) is associated to higher friction in most undoped systems, similar values of friction and interfacial distances between the C(110) and C(001) were obtained for the B-doped ones. Higher friction observed in the C(110) surfaces can be associated to the higher surface energy of this surface orientation (5.93 J/m^2 for the C(110), 5.91 J/m^2 for the reconstructed C(001) and 4.06 J/m^2 for the reconstructed C(111) surfaces [65]).

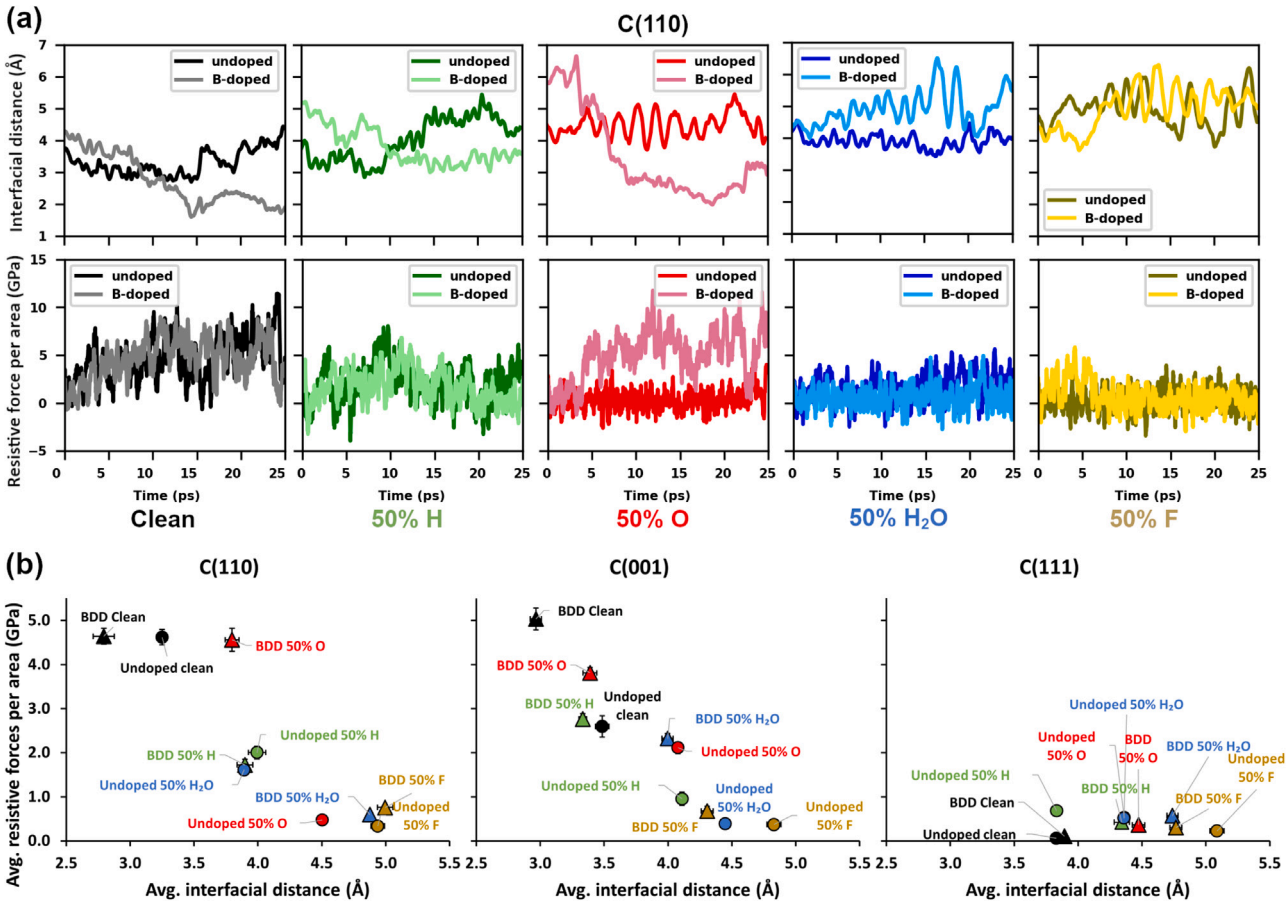

Fig. 3. (a): The evolution of the interfacial distance (top) and resistive forces per area (bottom) as a function of time for each of the considered surface passivations and the C(110) orientation. Dark (light) colors corresponds to the undoped (B-doped) systems. (b): Average resistive forces per area as a function of the average interfacial distance, for the C(110) (left), C(001) (middle) and C(111) (right) surfaces. Averaged quantities were calculated over 25 ps of sliding via the block averaging technique [64].

Interfacial adhesion has been shown to be proportional to the geometric average of the surface energies of the constituents [32], and the interfacial shear strength to be directly related, through a power law, to the interfacial adhesion [66]. The C(111) surfaces were found again to lead to the lowest friction values in all cases.

It is interesting to make a comprehensive list of the chemical events that occurred in each chemical environment and individually describe those that contribute most significantly to the aforementioned behaviors. Such discussion involves the results for the C(110) and C(001) surfaces alone, since no persistent breaking or forming of bonds were observed in all other cases where the C(111) surface was involved.

3.2.1. Clean surfaces

In the case of the clean, unpassivated diamond surfaces, chemical bonding interactions were consistently more pronounced compared to the systems with any type of passivating species, thus leading to the highest friction and smallest interfacial distance values. Specifically, in the C(110) surfaces, in both the undoped and the B-doped surfaces, the chemical interactions were triggered by the detachment of a H atom from a OH termination in silica and its migration on top of a C atom. The remaining silica terminations subsequently formed Si-O-C bonds with unpassivated C atoms on the diamond surface. These chemical events took place at very early times, already during the initial thermalization phase. Then, right after turning on the sliding velocity, further terminating OH groups from silica were fully dissociated on diamond, leading to multiple Si-C, Si-O-C and Si-O-B interactions (Fig. 5a, f). These resulted in turn in the pulling and, in some cases, in the detachment from the surface of C and B atoms, i.e., an initial wear stage of the diamond surface. This effect was more pronounced in the B-doped systems, as both B and C atoms were detached. However, while the B atom was subsequently adsorbed on the silica slab, displaced surface C atoms re-attached onto diamond surface sites in all cases (Fig. 5(a, f)). This observation is in agreement with another recent DFT study by our group, that has demonstrated that B doping favors the detachment of isolated B surface atoms, while C detachment from the undoped clean diamond surface occurs favorably via chain formation [67].

Similar interactions were also observed in the C(001) surfaces, however they start occurring after $\sim$ 2 ps of sliding in the B-doped, but only $\sim$ 10 ps of sliding in the undoped system (Fig. 5(k, p)). Moreover, no pronounced displacement or detachment of surface atoms was observed, verifying previous evidence that the C(110) surface is more prone to wear [68]. The higher surface energy of the C(110) surface [65] could also be correlated to the more pronounced tribochemical interactions observed in this case, which subsequently lead to wear.

3.2.2. 50% H termination

The mechanism of OH dissociation was also prevalent in the case of partially H-terminated diamond surfaces, leading again to Si-O-C/B and Si-C/B bridges between silica and unpassivated diamond surface sites, leading to the detachment of a surface B atom after $\sim$ 8 ps and its subsequent adsorption on the silica slab in the B-doped C(110) system (Fig. 5(g)). In the C(001) system, lower friction was observed in the undoped case, as full OH groups were formed on diamond unpassivated sites, creating an effective passivation that prevented strong bond formation with silica (Fig. 5(l)).

Also, in all cases, the oxidation of diamond surfaces was observed with the formation of C=O and C-O-C surface groups during sliding (Fig.

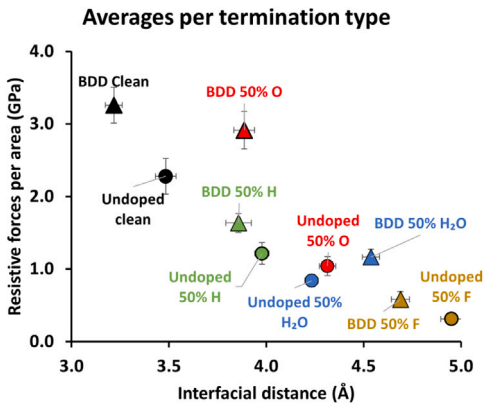

Fig. 4. Averages of Fig. 3(b) per termination type, over all three surface orientations. Black, green, red, blue and yellow notation corresponds to the systems involving clean and 50% H-, O-, split H_2O- and F-terminated diamond surfaces, respectively, while circles (triangles) denote systems involving undoped (B-doped) diamond surfaces.

5(b, g, l, q)). This effect was already reported in previous computational studies [23,45]. Oxidating agents have been traditionally used as an intermediate step for facilitating diamond polishing by weakening the surface and promoting the formation of cracks [69]. Here, it is more clearly observed that these O groups onto the diamond surface can act as anchoring points to the sliding silica surface and promote strong interactions at the interface.

3.2.3. 50% O termination

In the partially O-terminated systems, the impact of B doping was also particularly pronounced. In the undoped systems, as shown in Fig. 5(c, m), the dissociation of OH silica terminations which was identified as a driving mechanism for the interactions in the previous cases, was also observed either sparsely towards the final steps of sliding in the C(110) system, or leading to further passivation of the diamond surface and to the formation of a relatively limited number of Si-O-C and Si-C transient bonds, mostly at unpassivated sites in the C(001) system.

On the other hand, in the B-doped systems, OH dissociation events were present already during the initial thermalization phase and increased under sliding, leading to a large number of Si-C/B and Si-O-C/B strong interactions and resulting again in the displacement and detachment of uppermost C and B atoms from the C(110) surface (Fig. 5(h, r)).

3.2.4. 50% H_2O termination

Overall, the partial passivation with H and OH species was found to be among the most effective in reducing the strength of interfacial interactions. Specifically, in both the B-doped C(110) and C(001) surfaces, water fragments from the diamond terminations were recombined, forming H_2O molecules attached on diamond surface sites (Fig. 5 (i, s)). The beneficial role of B doping to the chemisorption of water molecules on diamond due to the promotion of the formation of dative B-O bonds in B-doped diamond surfaces has indeed been also reported by previous computational studies [57,58]. In both C(110) and C(001) surfaces, these chemisorbed water molecules induced a steric effect and limited bond formation with silica.

However, surface orientation played an important role in this system. In particular, on the B-doped C(110) surface, due to the flat geometry of the system, surface water groups were formed by the reorientation of neighboring OH terminating species on the diamond surface, as shown in Fig. 5(i). On the contrary, on the B-doped C(001) surface, governed by the rougher C=C dimer chain trenches, the surface water groups were formed by the adsorption of H from silica OH termination on diamond, leaving active Si-O species at the silica surface. This effect promoted stronger interfacial interactions and therefore mitigated the effect of the passivating water molecules in this case (Fig. 5(s)). Overall, it has been shown that B atoms enhance the adhesion of several different metallic interfaces [32] and also metal–diamond interface [33] suggesting that B atoms possess a universal character of adhesion enhancer. This is consistent with the increase of adhesion and friction observed in the present work for all the passivating species and not just for the OH-terminated ones as expected from the results of previous *ab initio* calculations [57,58,71].

3.2.5. 50% F termination

Partial F termination was found to consistently lower diamond–silica interactions more than the other terminating species considered in this study. However, a number of chemical events was still observed.

In the undoped surfaces, the dissociation of OH silica terminations on unpassivated diamond surface sites was observed, while F atoms from diamond were subsequently adsorbed on silica, replacing the missing OH terminations. However these events occurred only after 10–15 ps of sliding, with mostly non bonded physical interactions taking place for most of the considered sliding duration (Fig. 5(e, o)). The bond dissociation energies at 298 K for C-F and Si-F are 536 and 540 kj/mol, respectively [72], so F atoms are slightly more likely to form stable bonds with Si than with C. This can explain the tendency of F to be adsorbed on silica and to passivate the exposed Si atoms. The corresponding energies for C-H and Si-H are, respectively, 337 and 299 kj/mol [72]. This is also in agreement with previous studies reporting improved stability of the F terminations over the H ones and the strong repulsive interactions and low adhesion and friction associated with fluorination [18–21], but also shows that at the silica–diamond interface, F is more prone to bond to unpassivated Si than H.

On the other hand, the aforementioned reactions took place at the early stages of sliding in the B-doped systems and originated at the B unpassivated surface sites. In the C(001) surface, the initially unpassivated diamond sites were terminated with OH, H and C-O-C groups that in addition to the passivation of silica dangling bonds with F, reduced further bonding interactions at the interface (Fig. 5(t)).

Similar events occurred also in the C(110) system, with the exception that the initial OH dissociation resulted to a Si-O-B bridge that lead to the detachment of the B atom from diamond and its adsorption on silica. The adsorbed B atom was subsequently passivated with F atoms, also transferred to silica from diamond (Fig. 5(j)). It should be noted that in both B-doped surfaces, the main chemical events occurred within the first ~ 8 ps of sliding, with non-bonding interactions mostly taking place thereafter for the rest of the simulation time.

4. Conclusions

In this work, we performed large scale AIMD calculations for exploring the effects of different diamond passivations and B doping on the nanotribochemical interactions at the diamond–silica sliding interface under load, which are of high relevance in a plethora of technological applications. The C(110), the dimer-reconstructed C(001) and the Pandey-reconstructed C(111) surface orientations were considered, either clean or partially terminated with H, O, split H_2O (H+OH) and F species at 50% coverage.

The Pandey-reconstructed C(111) surfaces exhibited the most effective interfacial separation, as in these systems, only weak, non-bonding, physical interactions were observed throughout the entire simulation under sliding. On the contrary, the C(110) surfaces were found to be more prone to wear, with detachment of surface atoms from diamond observed in most cases. This can be correlated to the higher surface energy associated to this surface orientation [65].

The stronger interactions in most interfaces were found to originate from the initial dissociation of OH termination species from silica, leading to the creation of Si-O-C/B and Si-C/B bridges.

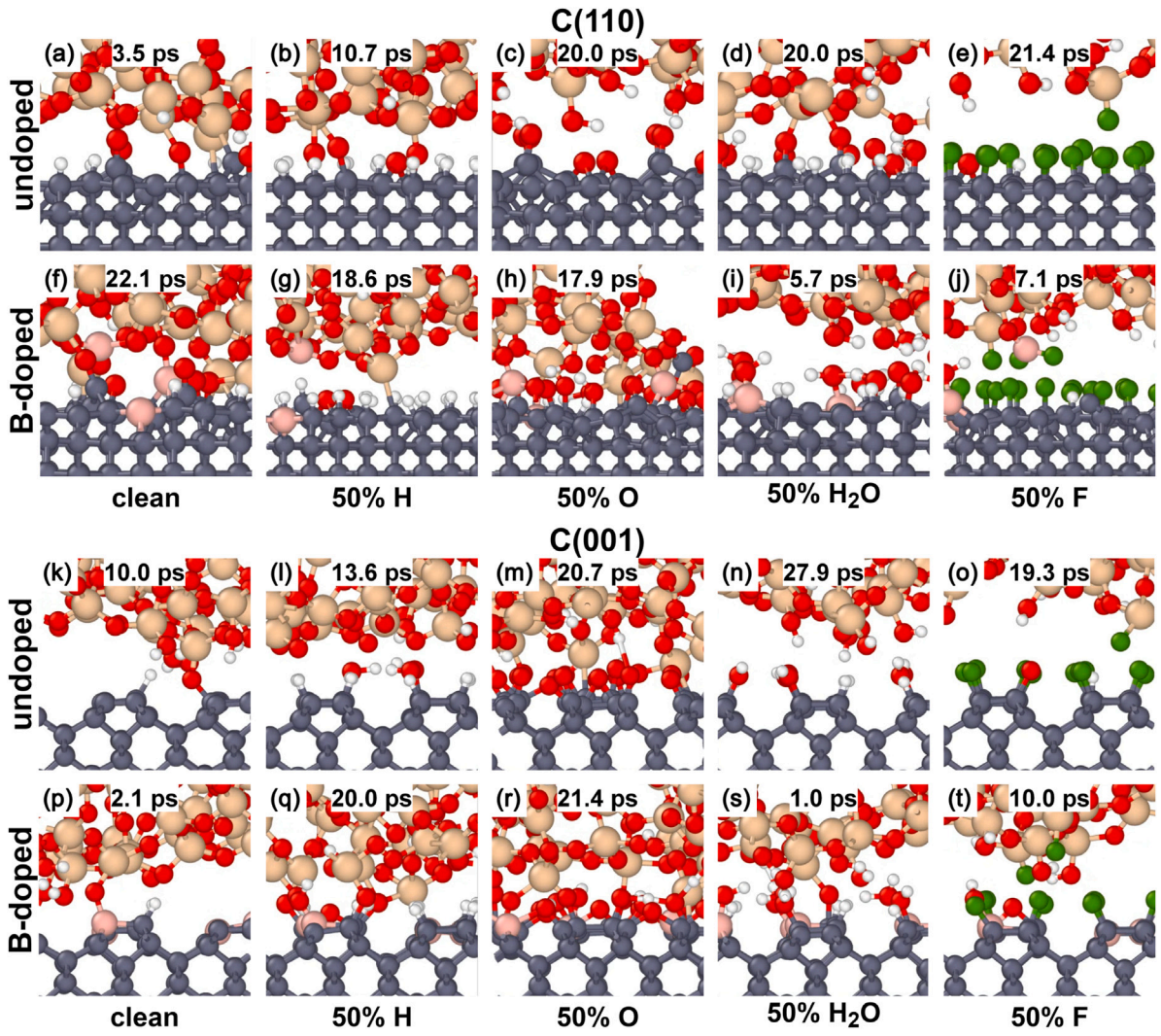

Fig. 5. Snapshots of the AIMD sliding calculations for the considered interfaces at selected timesteps. Color scheme: C: dark gray, B: pink, Si: yellow, H: white, O: red, F: green. The OVITO [70] package was used for the visualization of the dynamical atomic trajectories.

B doped diamond surfaces were associated to higher values of friction and smaller interfacial separations, as OH dissociation from silica on diamond surface sites was found to be promoted and to occur earlier on, compared to the respective undoped systems. Moreover, surface B atoms were found to be more prone to be detached from the surface compared to C.

F partial terminations lead consistently to the lowest friction forces and to the largest interfacial separations, followed by partial termination with water fragments. In the former case, the exchange of terminating species (F and OH) between diamond and silica was observed, leading to their re-passivation, while the effectiveness of the latter was found to be dependent on the surface orientation and B doping. On the other hand, clean surfaces were associated with the most pronounced amount of interactions at the interface due to the presence of dangling bonds. O partial terminations were found to be effective in passivating the interface mainly for the undoped surfaces, while in most cases H partial terminations showed inferior results in this context compared to the other considered passivating species. It should be noted that here we have considered a 50% passivation coverage in all cases, since previous calculations have shown that fully passivated surfaces are mostly governed by non-bonding interactions, yielding low adhesion and friction [14,22,23,59].

CRediT authorship contribution statement

Stefanos Giaremis: Writing – review & editing, Writing – original draft, Visualization, Validation, Methodology, Investigation, Formal analysis. **Huong Ta Thi Thuy:** Writing – review & editing, Writing – original draft, Visualization, Validation, Methodology, Investigation, Formal analysis. **Mauro Ferrario:** Writing – review & editing, Validation, Supervision, Software, Project administration, Methodology, Data curation. **Maria Clelia Righi:** Writing – review & editing, Validation, Supervision, Resources, Project administration, Methodology, Funding acquisition, Conceptualization.

Declaration of competing interest

The authors declare that they have no known competing financial interests or personal relationships that could have appeared to influence the work reported in this paper.

Acknowledgments

These results are part of the “Advancing Solid Interface and Lubricants by First-Principles Material Design (SLIDE)” project that has received funding from the European Research Council (ERC) under

the European Union's Horizon 2020 research and innovation program (Grant Agreement No. 865633). We acknowledge ISCRA for awarding this project access to the LEONARDO supercomputer, owned by the EuroHPC Joint Undertaking, hosted by CINECA (Italy). MCR acknowledges support by ICSC–Centro Nazionale di Ricerca in High Performance Computing, Big Data and Quantum Computing, funded by EuropeanUnion–NextGenerationEU.

Appendix A. Supplementary data

Supporting Information: Structural models of the relaxed diamond–silica interfaces for B-doped and undoped diamond at each of the considered surface orientations and terminations, under a load of 1 GPa applied on the topmost atoms of the silica slab, along with figures of interfacial distance and resistive force per area as a function of time, for each surface orientation and termination type (PDF). Animated representations of the full molecular dynamics trajectories (MP4).

Supplementary material related to this article can be found online at https://doi.org/10.1016/j.diamond.2025.112726.

Data availability

Data will be made available on request.

References

[1] K.A. Najar, N.A. Sheikh, M.M. Butt, S. Mushtaq, M.A. Shah, Engineered synthetic diamond film as a protective layer for tribological and machining applications: A review, J. Bio- Tribo-Corrosion 5 (3) (2019) 59, http://dx.doi.org/10.1007/s40735-019-0252-6.

[2] G. Li, M.Z. Rahim, W. Pan, C. Wen, S. Ding, The manufacturing and the application of polycrystalline diamond tools – a comprehensive review, J. Manuf. Process. 56 (2020) 400–416, http://dx.doi.org/10.1016/j.jmapro.2020.05.010.

[3] M. Liao, Progress in semiconductor diamond photodetectors and MEMS sensors, Funct. Diam. 1 (1) (2021) 29–46, http://dx.doi.org/10.1080/26941112.2021.1877019.

[4] A. Erdemir, M. Halter, G.R. Fenske, C. Zuiker, R. Csencsits, A.R. Krauss, D.M. Gruen, Friction and wear mechanisms of smooth diamond films during sliding in air and dry nitrogen, Tribol. Trans. 40 (4) (1997) 667–675, http://dx.doi.org/10.1080/10402009708983707.

[5] A. Mondelin, B. Furet, J. Rech, Characterisation of friction properties between a laminated carbon fibres reinforced polymer and a monocrystalline diamond under dry or lubricated conditions, Tribol. Int. 43 (9) (2010) 1665–1673, http://dx.doi.org/10.1016/j.triboint.2010.03.015.

[6] N. Kumar, N. Sharma, S. Dash, C. Popov, W. Kulisch, J. Reithmaier, G. Favaro, A. Tyagi, B. Raj, Tribological properties of ultrananocrystalline diamond films in various test atmosphere, Tribol. Int. 44 (12) (2011) 2042–2049, http://dx.doi.org/10.1016/j.triboint.2011.09.003.

[7] X. Liang, S. Zhang, L. Cui, M. Han, X. Yan, Friction and wear behaviors of polycrystalline diamond self-mated pairs in air and water lubrication conditions, Wear 530–531 (2023) 205006, http://dx.doi.org/10.1016/j.wear.2023.205006.

[8] A.R. Konicek, D.S. Grierson, P.U.P.A. Gilbert, W.G. Sawyer, A.V. Sumant, R.W. Carpick, Origin of ultralow friction and wear in ultrananocrystalline diamond, Phys. Rev. Lett. 100 (23) (2008) 235502, http://dx.doi.org/10.1103/physrevlett.100.235502.

[9] H. Kim, J. Lince, O. Eryilmaz, A. Erdemir, Environmental effects on the friction of hydrogenated DLC films, Tribol. Lett. 21 (1) (2006) 51–56, http://dx.doi.org/10.1007/s11249-005-9008-1.

[10] G. Zilibotti, S. Corni, M.C. Righi, Load-induced confinement activates diamond lubrication by water, Phys. Rev. Lett. 111 (14) (2013) 146101, http://dx.doi.org/10.1103/physrevlett.111.146101.

[11] T. Kuwahara, G. Moras, M. Moseler, Role of oxygen functional groups in the friction of water-lubricated low-index diamond surfaces, Phys. Rev. Mater. 2 (7) (2018) 073606, http://dx.doi.org/10.1103/physrevmaterials.2.073606.

[12] A. Erdemir, The role of hydrogen in tribological properties of diamond-like carbon films, Surf. Coat. Technol. 146–147 (2001) 292–297, http://dx.doi.org/10.1016/s0257-8972(01)01417-7.

[13] A. Erdemir, O. Eryilmaz, S. Kim, Effect of tribochemistry on lubricity of DLC films in hydrogen, Surf. Coat. Technol. 257 (2014) 241–246, http://dx.doi.org/10.1016/j.surfcoat.2014.08.002.

[14] M.-I. De Barros Bouchet, G. Zilibotti, C. Matta, M.C. Righi, L. Vandenbulcke, B. Vacher, J.-M. Martin, Friction of diamond in the presence of water vapor and hydrogen gas. coupling gas-phase lubrication and first-principles studies, J. Phys. Chem. C 116 (12) (2012) 6966–6972, http://dx.doi.org/10.1021/jp211322s.

[15] P. Manimunda, A. Al-Azizi, S.H. Kim, R.R. Chromik, Shear-induced structural changes and origin of ultralow friction of hydrogenated diamond-like carbon (dlc) in dry environment, ACS Appl. Mater. Interfaces 9 (19) (2017) 16704–16714, http://dx.doi.org/10.1021/acsami.7b03360.

[16] J. Fontaine, M. Belin, T. Le Mogne, A. Grill, How to restore superlow friction of DLC: the healing effect of hydrogen gas, Tribol. Int. 37 (11–12) (2004) 869–877, http://dx.doi.org/10.1016/j.triboint.2004.07.002.

[17] Y. Wang, K. Hayashi, Y. Ootani, S. Bai, T. Shimazaki, Y. Higuchi, N. Ozawa, K. Adachi, M.-I. De Barros Bouchet, J.M. Martin, M. Kubo, Role of OH termination in mitigating friction of diamond-like carbon under high load: A joint simulation and experimental study, Langmuir 37 (20) (2021) 6292–6300, http://dx.doi.org/10.1021/acs.langmuir.1c00727.

[18] F. Benini, P. Restuccia, M.C. Righi, Zinc dialkyldithiophosphates adsorption and dissociation on ferrous substrates: An ab initio study, Appl. Surf. Sci. 642 (2024) 158419, http://dx.doi.org/10.1016/j.apsusc.2023.158419.

[19] T. Reichenbach, L. Mayrhofer, T. Kuwahara, M. Moseler, G. Moras, Steric effects control dry friction of h- and f-terminated carbon surfaces, ACS Appl. Mater. Interfaces 12 (7) (2020) 8805–8816, http://dx.doi.org/10.1021/acsami.9b18019.

[20] S. Bai, T. Onodera, R. Nagumo, R. Miura, A. Suzuki, H. Tsuboi, N. Hatakeyama, H. Takaba, M. Kubo, A. Miyamoto, Friction reduction mechanism of hydrogen- and fluorine-terminated diamond-like carbon films investigated by molecular dynamics and quantum chemical calculation, J. Phys. Chem. C 116 (23) (2012) 12559–12565, http://dx.doi.org/10.1021/jp300937n.

[21] R. Prioli, L.G. Jacobsohn, M.E.H. Maia da Costa, F.L. Freire, Nanotribological properties of amorphous carbon-fluorine films, Tribol. Lett. 15 (3) (2003) 177–180, http://dx.doi.org/10.1023/A:1024848816646.

[22] H.T.T. Ta, N.V. Tran, M.C. Righi, Nanotribological properties of oxidized diamond/silica interfaces: Insights into the atomistic mechanisms of wear and friction by ab initio molecular dynamics simulations, ACS Appl. Nano Mater. 6 (18) (2023) 16674–16683, http://dx.doi.org/10.1021/acsanm.3c02881.

[23] M. Cutini, G. Forghieri, M. Ferrario, M.C. Righi, Adhesion, friction and tribochemical reactions at the diamond–silica interface, Carbon 203 (2023) 601–610, http://dx.doi.org/10.1016/j.carbon.2022.11.074.

[24] D. Kim, T. Fischer, B. Gallois, The effects of oxygen and humidity on friction and wear of diamond-like carbon films, Surf. Coat. Technol. 49 (1–3) (1991) 537–542, http://dx.doi.org/10.1016/0257-8972(91)90113-b.

[25] N.V. Tran, M. Righi, Ab initio insights into the interaction mechanisms between H_2 H_2O, and O_2 molecules with diamond surfaces, Carbon 199 (2022) 497–507, http://dx.doi.org/10.1016/j.carbon.2022.07.056.

[26] X. Li, L. He, Y. Li, Q. Yang, Catalytic graphite mechanism during cvd diamond film on iron and cobalt alloys in CH4-H2 atmospheres, Surf. Coat. Technol. 360 (2019) 20–28, http://dx.doi.org/10.1016/j.surfcoat.2018.12.120.

[27] K. Ramasubramanian, N. Arunachalam, M. Ramachandra Rao, Investigation on tribological behaviour of boron doped diamond coated cemented tungsten carbide for cutting tool applications, Surf. Coat. Technol. 332 (2017) 332–340, http://dx.doi.org/10.1016/j.surfcoat.2017.06.090.

[28] G. Skordaris, K.-D. Bouzakis, P. Charalampous, T. Kotsanis, E. Bouzakis, O. Lemmer, Effect of structure and residual stresses of diamond coated cemented carbide tools on the film adhesion and developed wear mechanisms in milling, CIRP Ann 65 (1) (2016) 101–104, http://dx.doi.org/10.1016/j.cirp.2016.04.007.

[29] S.H. Din, M. Shah, N. Sheikh, K. Najar, K. Ramasubramanian, S. Balaji, M. Ramachandra Rao, Influence of boron doping on mechanical and tribological properties in multilayer cvd-diamond coating systems, Bull. Mater. Sci. 39 (2016) 1753–1761.

[30] M. Lu, H. Wang, X. Song, F. Sun, Effect of doping level on residual stress, coating-substrate adhesion and wear resistance of boron-doped diamond coated tools, J. Manuf. Process. 88 (2023) 145–156, http://dx.doi.org/10.1016/j.jmapro.2023.01.041.

[31] M. Egiza, A.M. Ali, K. Murasawa, T. Yoshitake, B-doped nanodiamond composite hard coatings deposited on cemented carbide: Mechanical, structural, and tribological properties, Int. J. Refract. Met. Hard Mater. 114 (2023) 106260, http://dx.doi.org/10.1016/j.ijrmhm.2023.106260.

[32] E. Poli, M. Cutini, M. Nosir, O. Chehaimi, M. Righi, Effects of surface chemical modifications on the adhesion of metallic interfaces. an high-throughput first-principle analysis, Appl. Surf. Sci. 664 (2024) 160177, http://dx.doi.org/10.1016/j.apsusc.2024.160177.

[33] E. Damiani, M. Marsili, M.C. Righi, Tuning the adhesion of diamond/copper interfaces through surface chemical modifications and reconstruction, Carbon 230 (2024) 119555, http://dx.doi.org/10.1016/j.carbon.2024.119555.

[34] Z. Zhang, D. Xiang, Z. Zhang, Y. Zhang, B. Zhao, Study on tribology and cutting performance of boron doped diamond composite coated tool, Int. J. Refract. Met. Hard Mater. 117 (2023) 106385, http://dx.doi.org/10.1016/j.ijrmhm.2023.106385.

[35] S. Liza, J. Hieda, H. Akasaka, N. Ohtake, Y. Tsutsumi, A. Nagai, T. Hanawa, Deposition of boron doped dlc films on tinb and characterization of their mechanical properties and blood compatibility, Sci. Technol. Adv. Mater. 18 (1) (2017) 76–87, http://dx.doi.org/10.1080/14686996.2016.1262196.

[36] Q. Liang, A. Stanishevsky, Y.K. Vohra, Tribological properties of undoped and boron-doped nanocrystalline diamond films, Thin Solid Films 517 (2) (2008) 800–804, http://dx.doi.org/10.1016/j.tsf.2008.08.171.

[37] J.G. Buijnsters, M. Tsigkourakos, T. Hantschel, F.O.V. Gomes, T. Nuytten, P. Favia, H. Bender, K. Arstila, J.-P. Celis, W. Vandervorst, Effect of boron doping on the wear behavior of the growth and nucleation surfaces of micro- and nanocrystalline diamond films, ACS Appl. Mater. Interfaces 8 (39) (2016) 26381–26391, http://dx.doi.org/10.1021/acsami.6b08083.

[38] S.-F. Wang, Y.-F. Hsu, F.-C. Ku, Z.-Y. Liu, The effects of boron dopant on the thermal stability, semiconductor characteristic and wear resistance of diamond films, Mater. Res. Innov. 21 (6) (2016) 358–366, http://dx.doi.org/10.1080/14328917.2016.1265244.

[39] M. Lu, D. Liu, C. Zhang, F. Sun, Fabrication and high-temperature tribological performance of doped diamond film with b, n, and si elements, Ceram. Int. 50 (2) (2024) 2588–2599, http://dx.doi.org/10.1016/j.ceramint.2023.10.189.

[40] E.L. Thomas, G.W. Nelson, S. Mandal, J.S. Foord, O.A. Williams, Chemical mechanical polishing of thin film diamond, Carbon 68 (2014) 473–479, http://dx.doi.org/10.1016/j.carbon.2013.11.023.

[41] E.L.H. Thomas, S. Mandal, E.B. Brousseau, O.A. Williams, Silica based polishing of 100 and 111 single crystal diamond, Sci. Technol. Adv. Mater. 15 (3) (2014) 035013, http://dx.doi.org/10.1088/1468-6996/15/3/035013.

[42] L. Pastewka, S. Moser, P. Gumbsch, M. Moseler, Anisotropic mechanical amorphization drives wear in diamond, Nat. Mater. 10 (1) (2010) 34–38, http://dx.doi.org/10.1038/nmat2902.

[43] A. Peguiron, G. Moras, M. Walter, H. Uetsuka, L. Pastewka, M. Moseler, Activation and mechanochemical breaking of C–C bonds initiate wear of diamond (110) surfaces in contact with silica, Carbon 98 (2016) 474–483, http://dx.doi.org/10.1016/j.carbon.2015.10.098.

[44] K. Kawaguchi, Y. Wang, J. Xu, Y. Ootani, Y. Higuchi, N. Ozawa, M. Kubo, Atom-by-atom and sheet-by-sheet chemical mechanical polishing of diamond assisted by oh radicals: A tight-binding quantum chemical molecular dynamics simulation study, ACS Appl. Mater. Interfaces 13 (34) (2021) 41231–41237, http://dx.doi.org/10.1021/acsami.1c09468.

[45] X. Guo, S. Yuan, X. Wang, Z. Jin, R. Kang, Atomistic mechanisms of chemical mechanical polishing of diamond (1 0 0) in aqueous h2o2/pure h2o: Molecular dynamics simulations using reactive force field (reaxff), Comput. Mater. Sci. 157 (2019) 99–106, http://dx.doi.org/10.1016/j.commatsci.2018.10.041.

[46] T.D.B. Jacobs, J.A. Lefever, R.W. Carpick, Measurement of the length and strength of adhesive interactions in a nanoscale silicon–diamond interface, Adv. Mater. Interfaces 2 (9) (2015) 1400547, http://dx.doi.org/10.1002/admi.201400547.

[47] Z.B. Milne, J.D. Schall, T.D. Jacobs, J.A. Harrison, R.W. Carpick, Covalent bonding and atomic-level plasticity increase adhesion in silicon–diamond nanocontacts, ACS Appl. Mater. Interfaces 11 (43) (2019) 40734–40748, http://dx.doi.org/10.1021/acsami.9b08695.

[48] P. Giannozzi, S. Baroni, N. Bonini, M. Calandra, R. Car, C. Cavazzoni, D. Ceresoli, G.L. Chiarotti, M. Cococcioni, I. Dabo, A.D. Corso, S. de Gironcoli, S. Fabris, G. Fratesi, R. Gebauer, U. Gerstmann, C. Gougoussis, A. Kokalj, M. Lazzeri, L. Martin-Samos, N. Marzari, F. Mauri, R. Mazzarello, S. Paolini, A. Pasquarello, L. Paulatto, C. Sbraccia, S. Scandolo, G. Sclauzero, A.P. Seitsonen, A. Smogunov, P. Umari, R.M. Wentzcovitch, Quantum espresso: a modular and open-source software project for quantum simulations of materials, J. Phys.: Condens. Matter. 21 (39) (2009) 395502, http://dx.doi.org/10.1088/0953-8984/21/39/395502.

[49] P. Giannozzi, O. Andreussi, T. Brumme, O. Bunau, M.B. Nardelli, M. Calandra, R. Car, C. Cavazzoni, D. Ceresoli, M. Cococcioni, N. Colonna, I. Carnimeo, A.D. Corso, S. de Gironcoli, P. Delugas, R.A. DiStasio, A. Ferretti, A. Floris, G. Fratesi, G. Fugallo, R. Gebauer, U. Gerstmann, F. Giustino, T. Gorni, J. Jia, M. Kawamura, H.-Y. Ko, A. Kokalj, E. Küçükbenli, M. Lazzeri, M. Marsili, N. Marzari, F. Mauri, N.L. Nguyen, H.-V. Nguyen, A.O. de-la Roza, L. Paulatto, S. Poncé, D. Rocca, R. Sabatini, B. Santra, M. Schlipf, A.P. Seitsonen, A. Smogunov, I. Timrov, T. Thonhauser, P. Umari, N. Vast, X. Wu, S. Baroni, Advanced capabilities for materials modelling with quantum ESPRESSO, J. Phys.: Condens. Matter. 29 (46) (2017) 465901, http://dx.doi.org/10.1088/1361-648X/aa8f79.

[50] K. Laasonen, R. Car, C. Lee, D. Vanderbilt, Implementation of ultrasoft pseudopotentials in ab initio molecular dynamics, Phys. Rev. B 43 (1991) 6796–6799, http://dx.doi.org/10.1103/PhysRevB.43.6796, URL https://link.aps.org/doi/10.1103/PhysRevB.43.6796.

[51] J.P. Perdew, K. Burke, M. Ernzerhof, Generalized gradient approximation made simple phys, Rev. Lett. 77 (1996) 3865–3868, http://dx.doi.org/10.1103/PhysRevLett.77.3865, URL https://link.aps.org/doi/10.1103/PhysRevLett.77.3865.

[52] J.P. Perdew, K. Burke, M. Ernzerhof, Generalized gradient approximation made simple [phys. rev. lett. 77, 3865 (1996)],, Phys. Rev. Lett. 78 (1997) 1396, http://dx.doi.org/10.1103/PhysRevLett.78.1396, URL https://link.aps.org/doi/10.1103/PhysRevLett.78.1396.

[53] S. Grimme, Semiempirical GGA-type density functional constructed with a long-range dispersion correction, J. Comput. Chem. 27 (15) (2006) 1787–1799, http://dx.doi.org/10.1002/jcc.20495, arXiv:https://onlinelibrary.wiley.com/doi/pdf/10.1002/jcc.20495 URL https://onlinelibrary.wiley.com/doi/abs/10.1002/jcc.20495.

[54] V. Barone, M. Casarin, D. Forrer, M. Pavone, M. Sambi, A. Vittadini, Role and effective treatment of dispersive forces in materials: Polyethylene and graphite crystals as test cases, J. Comput. Chem. 30 (6) (2009) 934–939, http://dx.doi.org/10.1002/jcc.21112, arXiv:https://onlinelibrary.wiley.com/doi/pdf/10.1002/jcc.21112, URL https://onlinelibrary.wiley.com/doi/abs/10.1002/jcc.21112.

[55] T. Kunze, M. Posselt, S. Gemming, G. Seifert, A.R. Konicek, R.W. Carpick, L. Pastewka, M. Moseler, Wear, plasticity, and rehybridization in tetrahedral amorphous carbon, Tribol. Lett. 53 (1) (2013) 119–126, http://dx.doi.org/10.1007/s11249-013-0250-7.

[56] S. Turner, Y.-G. Lu, S.D. Janssens, F. Da Pieve, D. Lamoen, J. Verbeeck, K. Haenen, P. Wagner, G. Van Tendeloo, Local boron environment in b-doped nanocrystalline diamond films, Nanoscale 4 (19) (2012) 5960, http://dx.doi.org/10.1039/c2nr31530k.

[57] C. Ayestarán Latorre, J.P. Ewen, D. Dini, M. Righi, Ab initio insights into the interaction mechanisms between boron, nitrogen and oxygen doped diamond surfaces and water molecules, Carbon 171 (2021) 575–584, http://dx.doi.org/10.1016/j.carbon.2020.09.044.

[58] S. Giaremis, M.C. Righi, Tuning the adsorption of H_2O, H_2 and O_2 molecules on diamond surfaces by B-doping, Surf. Interfaces 46 (2024) 104105, http://dx.doi.org/10.1016/j.surfin.2024.104105.

[59] G. Zilibotti, M.C. Righi, Ab initio calculation of the adhesion and ideal shear strength of planar diamond interfaces with different atomic structure and hydrogen coverage, Langmuir 27 (11) (2011) 6862–6867, http://dx.doi.org/10.1021/la200783a.

[60] P. Vashishta, R.K. Kalia, J.P. Rino, I. Ebbsjö, Interaction potential for sio_2: A molecular-dynamics study of structural correlations, Phys. Rev. B 41 (17) (1990) 12197–12209, http://dx.doi.org/10.1103/physrevb.41.12197.

[61] A. Kokalj, Xcrysden—a new program for displaying crystalline structures and electron densities, J. Mol. Graph. Model. 17 (3–4) (1999) 176–179, http://dx.doi.org/10.1016/s1093-3263(99)00028-5.

[62] A. Kailer, K.G. Nickel, Y.G. Gogotsi, Raman microspectroscopy of nanocrystalline and amorphous phases in hardness indentations, J. Raman Spectrosc. 30 (10) (1999) 939–946, http://dx.doi.org/10.1002/(sici)1097-4555(199910)30:10<939::aid-jrs460>3.0.co;2-c.

[63] F. Katsuki, A. Saguchi, W. Takahashi, J. Watanabe, The atomic-scale removal mechanism during si tip scratching on si and SiO2 surfaces in aqueous KOH with an atomic force microscope, Japan. J. Appl. Phys. 41 (Part 1, No. 7B) (2002) 4919–4923, http://dx.doi.org/10.1143/jjap.41.4919.

[64] C. Templeton, R. Elber, M. Ferrario, G. Ciccotti, A new boundary driven NEMD scheme for heat and particle diffusion in binary mixtures, Mol. Phys. 119 (19–20) (2021) e1892849, http://dx.doi.org/10.1080/00268976.2021.1892849.

[65] A.A. Stekolnikov, J. Furthmüller, F. Bechstedt, Absolute surface energies of group-iv semiconductors: Dependence on orientation and reconstruction, Phys. Rev. B 65 (11) (2002) http://dx.doi.org/10.1103/physrevb.65.115318.

[66] M. Wolloch, G. Losi, M. Ferrario, M.C. Righi, High-throughput screening of the static friction and ideal cleavage strength of solid interfaces, Sci. Rep. 9 (1) (2019) http://dx.doi.org/10.1038/s41598-019-49907-2.

[67] S. Giaremis, M.C. Righi, Exploring atomistic wear mechanisms in b-doped diamond surfaces via ab initio calculations, Tribol. Int. 204 (2025) 110438, http://dx.doi.org/10.1016/j.triboint.2024.110438.

[68] H.T.T. Ta, N.V. Tran, M.C. Righi, Atomistic wear mechanisms in diamond: Effects of surface orientation, stress, and interaction with adsorbed molecules, Langmuir 39 (40) (2023) 14396–14403, http://dx.doi.org/10.1021/acs.langmuir.3c01800.

[69] A. Malshe, B. Park, W. Brown, H. Naseem, A review of techniques for polishing and planarizing chemically vapor-deposited (CVD) diamond films and substrates, Diam. Relat. Mater. 8 (7) (1999) 1198–1213, http://dx.doi.org/10.1016/s0925-9635(99)00088-6.

[70] A. Stukowski, Visualization and analysis of atomistic simulation data with ovito–the open visualization tool, Modelling Simul. Mater. Sci. Eng. 18 (1) (2009) 015012, http://dx.doi.org/10.1088/0965-0393/18/1/015012.

[71] S. Peeters, T. Kuwahara, F. Härtwig, S. Makowski, V. Weihnacht, A.F. Lasagni, M. Dienwiebel, M. Moseler, G. Moras, Surface depassivation via B–o dative bonds affects the friction performance of B-doped carbon coatings, ACS Appl. Mater. Interfaces 16 (14) (2024) 18112–18123, http://dx.doi.org/10.1021/acsami.3c18803.

[72] N.A. Lange, Lange's Handbook of Chemistry, fifteenth ed., McGraw-Hill, New York, NY, 1999.